

DUST-COOLING-INDUCED FRAGMENTATION OF LOW-METALLICITY CLOUDS

TORU TSURIBE¹ AND KAZUYUKI OMUKAI²

To appear in The Astrophysical Journal Letters.

ABSTRACT

Dynamical collapse and fragmentation of low-metallicity cloud cores is studied using three-dimensional hydrodynamical calculations, with particular attention devoted whether the cores fragment in the dust-cooling phase or not. The cores become elongated in this phase, being unstable to non-spherical perturbation due to the sudden temperature decrease. In the metallicity range of $10^{-6} - 10^{-5}Z_{\odot}$, cores with an initial axis ratio $\gtrsim 2$ reach a critical value of the axis ratio ($\gtrsim 30$) and fragment into multiple small clumps. This provides a possible mechanism to produce low-mass stars in ultra-metal-poor environments.

Subject headings: cosmology: theory — hydrodynamics — instabilities — stars: formation

1. INTRODUCTION

It has been suggested that the first stars in the universe were very massive, typically $\gtrsim 100M_{\odot}$ (e.g., Abel, Bryan, & Norman 2000, 2002; Bromm et al. 1999, 2002; Omukai & Palla 2001, 2003). On the other hand, in present-day local star-forming regions, typical stars are low-mass objects $\lesssim 1M_{\odot}$. One of the major factors distinguishing these two modes of star formation is the degree of metal enrichment. At some point in the history of the universe, metallicity exceeds a critical value and the transition to low-mass star formation mode is thought to take place. Since the exact value of critical metallicity is crucial in modeling such important problems as galaxy formation and reionization of the intergalactic medium etc., some authors have tried to establish this value. Bromm, Ferrara, Coppi & Larson (2001) studied the fragmentation of low-metallicity clouds, and concluded that clouds with metallicity $\gtrsim 5 \times 10^{-4}Z_{\odot}$ fragment into smaller pieces owing to the fine-structure line cooling of carbon and oxygen. Taking into account possible variations in the elemental abundance ratio, Bromm & Loeb (2003) derived individual critical abundances of C^{+} and O. Santoro & Shull (2005) included silicon and iron in a similar analysis. However, due to limitations imposed by inclusion of only the atomic line cooling, these authors only studied the thermal evolution in the low-density regime. The mass scale of such fragments is still high $\gtrsim 10 - 100M_{\odot}$, and another phase of fragmentation is necessary to produce low-mass ($\lesssim 1M_{\odot}$) objects. Regarding this problem, based on the thermal evolution described by Omukai (2000), Schneider et al. (2002, 2003) pointed out that another episode of fragmentation can be caused by dust cooling at higher densities (say, $\gtrsim 10^{10}\text{cm}^{-3}$). They concluded that dust-induced fragmentation can take place even with metallicity of $10^{-5\pm 1}Z_{\odot}$ and this produces low-mass ($\lesssim 1M_{\odot}$) fragments. However, their treatment of dynamical evolution was too simple and their prediction of fragmentation remained speculative.

In the previous paper (Omukai et al. 2005), using an updated thermal evolution and the linear theory for growth of elongation (Hanawa & Matsumoto 2000), we evaluated fragmentation mass scale under the assumption that fragmentation takes place when the elongation exceeds a critical value (~ 1) in the linear theory. However, an approximately spheri-

cal core, for which the linear theory is applicable, is not subject to fragmentation. Only a highly elongated, filamentary (or disk-like) object is gravitationally unstable and easily fragments (e.g., Larson 1995; Tsuribe & Inutsuka 1999b). Consequently, a discussion based on linear theory needs to be justified by numerical calculations.

In consideration of the above, here we follow the evolution of low-metallicity cores during the dust-cooling phase using three-dimensional hydrodynamical calculations and discuss the conditions for fragmentation into low-mass clumps. Our results confirm that the previous analysis by Omukai et al. (2005) is broadly correct: fragmentation does occur in the dust-cooling phase and sub-solar mass fragments are indeed produced.

2. NUMERICAL MODELING

H₂-line cooling induces fragmentation of low-metallicity ($\lesssim 10^{-4}Z_{\odot}$) interstellar clouds around 10^4cm^{-3} , and cloud cores are produced. Subsequently, the cores start a so-called run-away collapse, where they contract at almost the free-fall rate. Here we study evolution of such cores using three-dimensional hydrodynamical calculation. Since the cores are already self-gravitating, the dark-matter gravity is not considered. For simplicity, the cores are assumed to be non-rotating and isolated.

During the run-away collapse phase, a metal-free pre-stellar core obeys the self-similar flow with $\gamma \simeq 1.1$, as indicated by one-dimensional radiation hydrodynamical calculations (Omukai & Nishi 1998). Here we choose such a self-similar solution as an unperturbed initial state. The initial central number density is 10^{10}cm^{-3} where the dust cooling is about to become effective.

We add both non-spherical density/velocity and random-velocity perturbations to the initial state. As a non-spherical density perturbation, the sphere is elongated to a prolate with expanding in the z -direction and shrinking in x - and y -directions homologously while the central density is kept constant. We adopt prolate elongation because we find that the initial oblateness leads the amplitude of elongation to saturation in the non-linear regime before fragmentation takes place. Elongation of the core is defined by $\mathcal{E}_0 = a/b - 1$, where a (b) is the short (long, respectively) core axis length. Here, cases with an initial elongation of $\mathcal{E}_0 = 0.1, 0.32, 0.56$, and 1.0 are considered. Non-spherical velocity perturbation is added to the unperturbed flow. The amplitude of non-spherical velocity perturbation is assumed to be proportional to the displace-

¹ Osaka University, Toyonaka, Osaka 540-0053, Japan; tsuribe@vega.ess.sci.osaka-u.ac.jp

² National Astronomical Observatory of Japan, Mitaka, Tokyo 181-8588, Japan; omukai@yso.mtk.nao.ac.jp

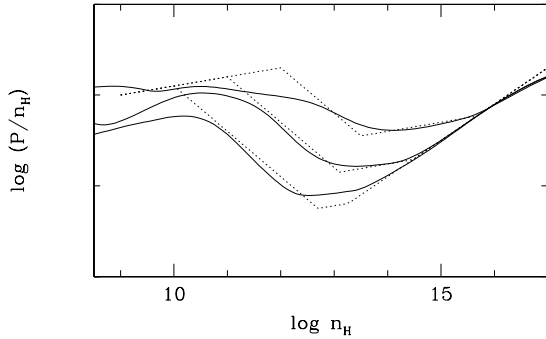


FIG. 1.— Effective equations of state (EOS) for clouds with $Z/Z_{\odot} = 10^{-6}, 10^{-5}$ and 10^{-4} (solid). Also shown (dashed) are approximate relations (eq. 1) used in the hydrodynamical calculation.

ment from the sphere and chosen so that the correct linear growth (or damping) rate is achieved. Additionally, a random velocity field with an amplitude of $0.1c_s$ is added, where c_s is the isothermal sound velocity at the center.

Solving full thermal equations along with hydrodynamics is numerically too expensive. Here we take the following simplified approach: First, using a one-zone model, we solve thermal and chemical processes under the assumption of free-fall collapse. The model is the same as in Omukai et al. (2005), except the dust model, for which we use dust produced by the pair-instability supernova of a metal-free $195M_{\odot}$ star (Schneider, Salvaterra, & Ferrara 2004; Schneider et al. 2006). The effective equations of state calculated with this model are shown in Figure 1 for metallicities $10^{-6}, 10^{-5}$, and $10^{-4}Z_{\odot}$. Next, for easier analysis and interpretation of the result, we approximate the above equations of state using the following barotropic relations: the ratio of specific heat $\gamma \equiv d \log p / d \log \rho$ is given by

$$\gamma = \begin{cases} 1.1 & (n < n_1) \\ 0.5 & (n_1 < n < n_2) \\ 1.1 & (n_2 < n < n_3) \\ 1.4 & (n_3 < n), \end{cases} \quad (1)$$

where $\log n_1 = 6 - \log Z/Z_{\odot}$, $\log n_2 = 11.1 - 0.4 \log Z/Z_{\odot}$, and $\log n_3 = 8.47 - 1.2 \log Z/Z_{\odot}$. In Figure 1, these relations are also shown by dotted lines. The first phase ($n < n_1$) corresponds to the H_2 -cooling phase, the second ($n_1 < n < n_2$) and third ($n_2 < n < n_3$) to the dust-cooling phase before and after the gas-dust coupling, and the last ($n_3 < n$) to the adiabatic contraction after the core becomes optically thick at n_3 .

Godunov-type smoothed particle hydrodynamics (SPH) with a second-order Riemann solver are used for hydrodynamics and a Tree method is used for gravitational force (Tsuribe & Inutsuka 1999a). The number of SPH particles is $N = 1.6$ (in Runs A, B, D, F, and G) or 2.3×10^6 (in Runs C and E), which is sufficiently large to meet the resolution condition for physical fragmentation (Klein et al 2004).

3. RESULTS

Major parameters in this model are the metallicity Z , which determines the equation of state, and the initial amplitude of elongation \mathcal{E}_0 . The numerical results can be classified into two types according to whether the core fragments or not. In the following, we show the typical models for these cases.

3.1. Cores with Fragmentation

Figure 2 shows the evolution of the core with $Z = 10^{-5}Z_{\odot}$ and $\mathcal{E}_0 = 1.0$. Initially, while the core is close to spherical, the evolution of elongation obeys the prediction by the linear analysis of a $\gamma = 1.1$ cloud. For central densities $n \gtrsim n_1 (= 10^{11} \text{cm}^{-3})$, the temperature decreases rapidly owing to the dust cooling, and the core collapses at almost the free-fall rate. In this phase, the elongation grows in proportion to ρ^m with $m = 0.354 - 0.5$, which is between the rate for spherical pressure-free collapse ($m = 0.354$) and that for filament collapse ($m = 0.5$). In other words, the rate m is enhanced from the linear value for a sphere owing to a non-linear effect. The equation of state begins to stiffen to $\gamma = 1.1$ at $n = n_2 (= 10^{13} \text{cm}^{-3})$, where the dust and gas couple thermally, and become adiabatic ($\gamma = 1.4$) at $n = n_3 (= 3 \times 10^{14} \text{cm}^{-3})$, where the core becomes optically thick. However, the core continues to elongate owing to inertia until $n \sim 10^{16} \text{cm}^{-3}$, where the maximum value of elongation $\mathcal{E}_{\text{max}} = 61$ is attained. A long spindle forms in the high-density core. Around this epoch, the spindle stops collapsing in a cylindrical radial direction and then fragments. Using the scale height of a filament $H = (2c_s^2/\pi G \bar{\rho}_c)^{1/2}$, where c_s and $\bar{\rho}_c$ is isothermal sound speed and density averaged over the z -axis, the interval between each fragment is well described by $2\pi H$, corresponding to maximum growing mode in the linear stability analysis of equilibrium filaments (Nagasawa 1987; Inutsuka & Miyama 1997). The filament fragments into four pieces. Since the fragments have an infall velocity along the z -axis, they merge with each other at the center, owing to small initial random velocities. This is partly because we do not include effects of rotation and angular momentum. In spite of the merging of fragments at the center, the number of fragments does not decrease, at least within the present calculation, since new fragments continue to be born on the outskirts. We also studied a case with the same parameters (Z, \mathcal{E}_0), but with a different seed for the random number. In this case, positions of density peaks were altered, but the distance between each fragment remained almost the same. The dynamical evolution was also similar.

In the case of lower metallicity ($Z = 10^{-6}Z_{\odot}$, $\mathcal{E}_0 = 1.0$), the maximum elongation becomes smaller ($\mathcal{E}_{\text{max}} \sim 40$) because of a weaker effect of dust cooling. Fragmentation is marginally observed. There are two fragments.

3.2. Cores without Fragmentation

Models with smaller initial elongation exhibit different evolution. As an example, we show one model with $Z = 10^{-5}Z_{\odot}$ and $\mathcal{E}_0 = 0.32$ in Figure 3. In the initial stage ($\gamma = 1.1$), the evolution of elongation is very similar to examples with fragmentation (§3.1). Subsequently, in the cooling phase ($n \gtrsim n_1 = 10^{11} \text{cm}^{-3}$), the elongation grows. The growth rate, however, remains close to the linear growth rate ($m = 0.354$) because of the small initial elongation. Then, the growth of elongation slows down at $n_3 \simeq 3 \times 10^{14} \text{cm}^{-3}$, where the equation of state becomes adiabatic. The maximum elongation reaches 14 in this case, but this is not enough to cause fragmentation. Thereafter, the core becomes more spherical with contraction, instead of becoming cylindrical. We also followed the evolution in the subsequent accretion stage by concentrating on the central region. No fragmentation was observed in our calculation.

In this calculation, the maximum value of axis ratio reaches 14. This exceeds both the critical value for fragmentation π and maximum growing mode 2π for fragmentation in the linear analysis for uniform infinite filaments. Despite this, the

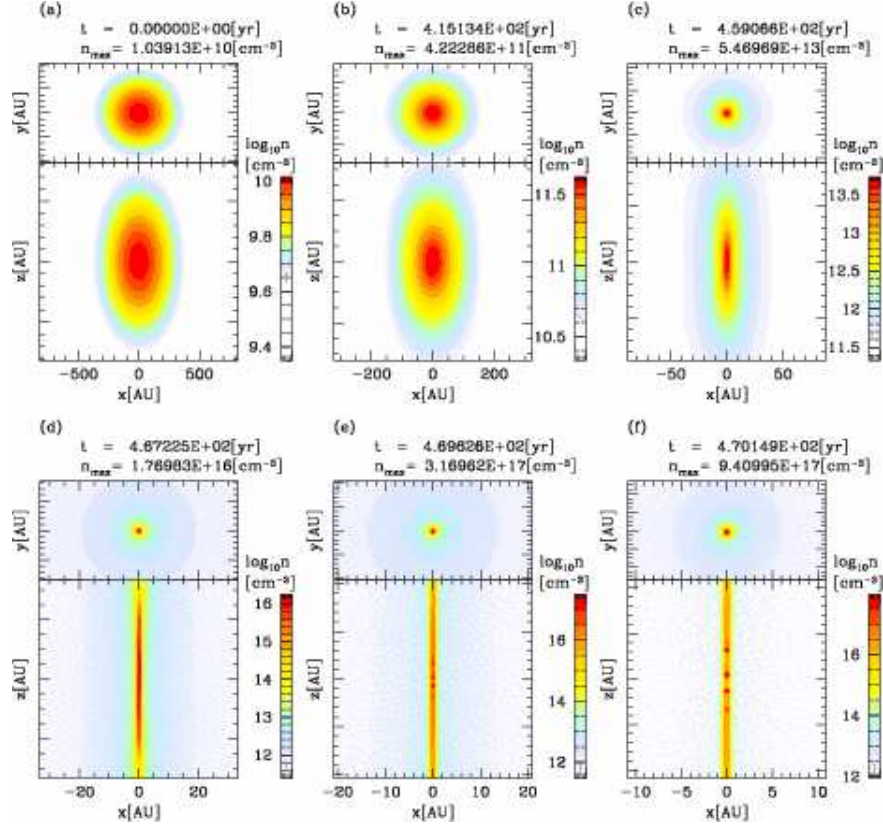


FIG. 2.— Density distribution in the x-y plane on the midplane (top panels), x-z plane of $y=0$ (bottom panels) for the case with $\mathcal{E}_0 = 1.0$ and $Z = 10^{-5}Z_{\odot}$ at six different stages. The color scale denotes the density in the logarithmic scale. The maximum number density and time are shown in each panel.

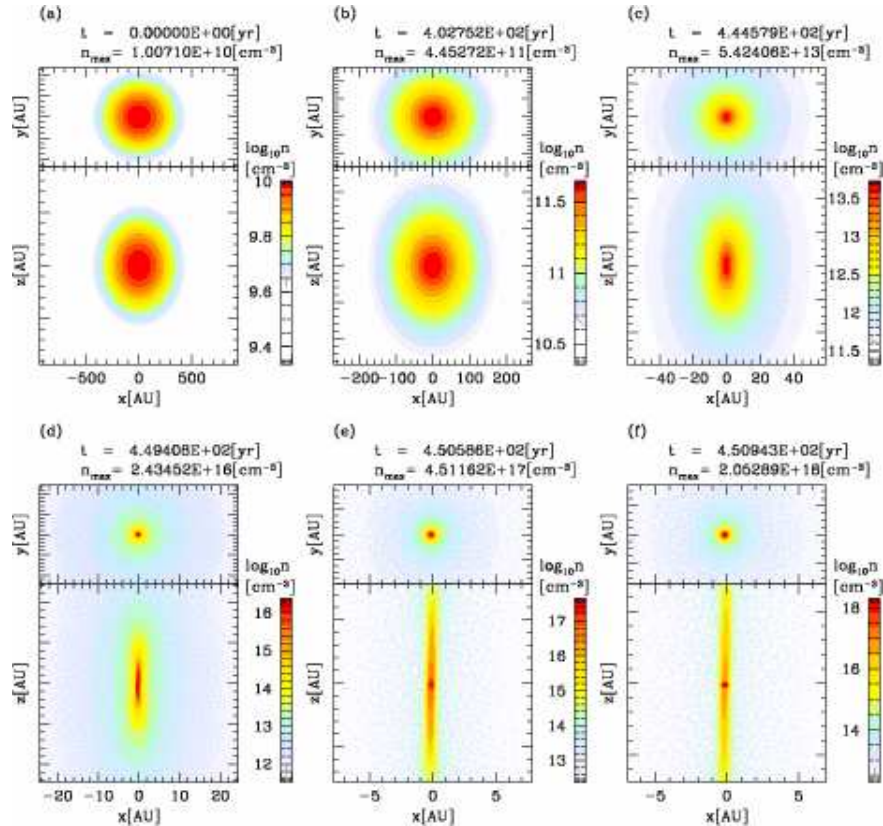


FIG. 3.— Same as Fig. 1 but for the case with $\mathcal{E}_0 = 0.32$ and $Z = 10^{-5}Z_{\odot}$.

TABLE 1
MODEL PARAMETERS AND RESULTS

| Run | $\log Z/Z_{\odot}$ | \mathcal{E}_0 | \mathcal{E}_{\max} | $\log n_{\max}$ | $\mathcal{E}_{\max,L}$ | Fragmentation |
|-----|--------------------|-----------------|----------------------|-----------------|------------------------|---------------|
| A | -6 | 0.56 | 16 | 16.8 | 1.5 | No |
| B | -6 | 1.0 | 30 | 16.6 | 2.7 | Yes |
| C | -5 | 0.32 | 14 | 16.4 | 1.6 | No |
| D | -5 | 0.56 | 27 | 16.1 | 2.8 | Yes |
| E | -5 | 1.0 | 61 | 16.0 | 4.9 | Yes |
| F | -4 | 0.32 | 34 | 15.6 | 2.9 | Yes |
| G | -4 | 0.56 | 56 | 15.3 | 5.1 | Yes |

NOTE: Model parameters are metallicity $\log Z/Z_{\odot}$ and the initial elongation \mathcal{E}_0 . \mathcal{E}_{\max} is the maximum value of elongation, which is attained at the number density n_{\max} . $\mathcal{E}_{\max,L}$ is the maximum value of elongation in the linear theory.

filament does not fragment because of the central density concentration in our case. Accretion onto the central density peak is faster than fragmentation on the outskirts. In the cases with $\mathcal{E}_0 = 0.1$, no fragmentation is observed for any of the metallicities.

4. CONCLUSION AND DISCUSSION

We have studied the fragmentation process of low-metallicity ($10^{-6} - 10^{-4}Z_{\odot}$) cloud cores at high densities ($\gtrsim 10^{10}\text{cm}^{-3}$). Cores with initial axis ratios greater than about two become elongated enough to fragment via dust-cooling, even with metallicities of $10^{-6} - 10^{-5}Z_{\odot}$. This provides a possible mechanism to produce low-mass stars in ultra-metal-deficient environments. The results of our calculations are summarized in Table 1. As a rule of thumb, fragmentation takes place if the core elongation reaches a critical value $\mathcal{E}_{\text{crit}} \gtrsim 30$. According to linear analysis for a filament of infinite length, namely, without density gradient along the long axis, an equilibrium filament is gravitationally unstable and subject to fragmentation if the axis ratio is greater than π (Nagasawa 1987). In our case, the filament is of finite length. The density gradient toward the center along the long axis makes the critical value for fragmentation several times larger than that for a filament of infinite length as discussed in §3.2. In Table 1, the maximum values of elongation in the linear analysis $\mathcal{E}_{\max,L}$ are also presented. We see that if $\mathcal{E}_{\max,L}$ exceeds ~ 3 , the elongation of the core will eventually reach $\mathcal{E}_{\text{crit}} \gtrsim 30$ and the core fragments. It should be noted that the actual maximum value of elongation and that in linear theory are not reached at the same time because of non-linear effects. The linear maximum value of elongation $\mathcal{E}_{\max,L}$ is attained at the

end of the rapid dust-cooling phase (i.e., $n = n_2$), since the elongation grows (or decays) if $\gamma < 1.09$ ($\gamma > 1.09$, respectively), in the linear theory (Hanawa & Matsumoto 2000; Lai 2000). On the other hand, the actual maximum is reached slightly after the core becomes adiabatic (i.e., $n \gtrsim n_3$).

Although we have demonstrated by detailed numerical work that dust-induced fragmentation indeed occurs under some circumstances, some points still remain to be improved. To avoid too large a dynamic range, we were forced to take the initial state of our calculation at a rather high density of 10^{10}cm^{-3} and parameterize the elongation of cores at this point. The question of how frequently such an initial condition is realized remains uncertain. The evolution after fragmentation is also to be studied. The final mass of stars is determined as a result of complex dynamical evolution such as merging and accretion. In this phase, angular momentum would play an important role, although we have neglected effects of rotation for simplicity. For example, a disk may fragment into multiples during the accretion phase (e.g., Saigo, Matsumoto, & Umemura 2004). These issues should be investigated in a future work.

Numerical computations were carried out on VPP5000 at the Astronomical Data Analysis Center of the National Astronomical Observatory of Japan and in the computational facilities at Osaka University. This research was supported in part by Grants-in-Aid for Young Scientists (B) 14740129 (TT) by the Ministry of Education, Culture, Sports, Science, and Technology of Japan (MEXT).

REFERENCES

- Abel, T., Bryan, G. L., & Norman, M. L. 2002, *Science*, 295, 93
 Bromm, V., Coppi, P. S., & Larson, R. B. 2002, *ApJ*, 564, 23
 Bromm, V., Ferrara, A., Coppi, P. S., & Larson, R. B. 1999, *MNRAS*, 328, 969
 Hanawa, T., & Matsumoto, T. 2000, *PASJ*, 52, 241
 Klein, R. I., Fisher, R., & McKee, C. F. 2004, *RMxAC*, 22, 3
 Lai, D. 2000, *ApJ*, 540, 946
 Larson, R. B. 1985, *MNRAS*, 214, 379
 Nagasawa, 1987, *Prog. Theor. Phys.*, 77, 635
 Omukai, K. 2000, *ApJ*, 534, 809
 Omukai, K. & Nishi, R. 1998, *ApJ*, 518, 64
 Omukai, K., Tsuribe, T., Schneider, R. & Ferrara, A. 2005, *ApJ*, 626, 627
 Saigo, K., Matsumoto, T., & Umemura, M. 2004, *ApJ*, 615, L65
 Santoro, F., & Shull, J. M. 2005, *ApJ*, submitted (astro-ph/0509101)
 Schneider, R., Ferrara, A., Natarajan, P., & Omukai, K. 2002, *ApJ*, 571, 30
 Schneider, R., Ferrara, A., Salvaterra, R., Omukai, K., & Bromm, V. 2003, *Nature*, 422, 869
 Schneider, R., Salvaterra, R., & Ferrara, A. 2004, *MNRAS*, 351, 1379
 Schneider, R., Inoue, A. K., Omukai, K., & Ferrara, A. 2006, in preparation
 Tsuribe, T. & Inutsuka, S. 1999, *ApJ*, 523, L155
 Tsuribe, T. & Inutsuka, S. 1999, *ApJ*, 526, 307